



Temperature induced immiscibility in the NaCl–H₂O system at high pressure

Mark R. Frank^{a,*}, Henry P. Scott^b, Steven J. Maglio^a, Vitali B. Prakapenka^c, Guoyin Shen^d

^a Department of Geology and Environmental Geosciences, Northern Illinois University, DeKalb, IL 60115, United States

^b Department of Physics and Astronomy, Indiana University South Bend, South Bend, IN 46634, United States

^c Center for Advanced Radiation Sources, University of Chicago, Chicago, IL 60637, United States

^d HPCAT, Geophysical Laboratory, Carnegie Institution of Washington, Argonne, IL 60439, United States

ARTICLE INFO

Article history:

Received 25 February 2008

Received in revised form 12 July 2008

Accepted 29 July 2008

Keywords:

High-pressure H₂O

Icy satellites

NaCl–H₂O

Immiscibility

Subsurface oceans

ABSTRACT

High-pressure polymorphs of H₂O are a major component in many outer planets, extra solar bodies, and icy satellites. This study sought to examine the influence of ionic impurities on the phase stability, thermal expansion, and melting curve of ice VII. Powder diffraction patterns of ice VII formed from pure H₂O and 5 wt.% NaCl aqueous solutions were taken at room temperature up to 11.1 ± 0.3 and 26.6 ± 0.4 GPa, respectively. Thermal expansions, α , of all ice VII samples were recorded and modeled up to the melting point of the samples. Ice VII formed from a NaCl-bearing aqueous solution at pressures greater than 2.2 GPa and less than 500 K can be indexed by ice VII only, whereas at temperatures greater than 500 K, diffraction lines indicative of halite (NaCl) are observed and become more intense with increasing temperature and only disappear at the melting point of the high-pressure ice. This phenomenon was observed in all NaCl-bearing ice samples that were heated to greater than 500 K. The melting curves of ice VII formed from pure H₂O and a 5 wt.% NaCl aqueous solution suggest that the presence of Na⁺ and Cl⁻ in the ice VII structure results in a depression of the melting curve by approximately 40 K. The exsolution of halite from the NaCl-doped ice VII and the depression of the ice VII melting curve suggest that the presence of ionic impurities in ice VII may promote the formation of a self-segregating zone deep within ice-rich bodies. This zone could initiate the formation of solute-rich melt pockets that may ascend toward the surface and result in surface manifestations such as solute-bearing aqueous vents, unexplained domes/diapirism, and/or salt-rich regions.

© 2008 Elsevier B.V. All rights reserved.

1. Introduction

High-pressure phases of H₂O, specifically ice VI, VII and X, have been hypothesized to make up a significant portion of the interiors of select outer planets, extra solar bodies, the Galilean satellites, and Saturn's Titan (Consolmagno and Lewis, 1976; Anderson et al., 1996, 1997, 2001; Carlson et al., 1996; Kivelson et al., 1996; Schubert et al., 1996; Khurana et al., 1998; McCord et al., 1998; Brown and Calvin, 2000; Greeley et al., 2000a, 2000b; Zimmer et al., 2000; McCord et al., 2001; Schenk et al., 2001; Head et al., 2002). For example, Gliese 436 b (or GJ 436 b), discovered in 2004 (Butler et al., 2004), is a Neptune-sized body orbiting the star GJ 436. The planet's density falls between hydrogen-rich gas giants (like Jupiter) and the terrestrial planets. Its semi-major axis is less than 10% that of Mercury; thus, the surface of GJ 436 b is very hot with temperatures ranging from 650 K on the daylight side to as low as 475 K on a possibly tidally locked night side. Gillon et al. (2007) estimated the

planet's diameter as $50.4 \pm 4.5 \times 10^3$ km and suggested that the vast majority of its interior is composed of solid H₂O phases stable at elevated temperatures (an alternative to this model is a terrestrial core surrounded by gas). The two most likely phases within the body are ice VII and ice X which, at room temperature, are stable from 2.2 to 62 GPa and at pressures greater than 62 GPa, respectively. Ice VII has a body-centered cubic structure with disordered hydrogen bonding through the water hexamers, whereas ice X has protons which are equidistant between the oxygen atoms (Pruzan et al., 1997; Goncharov et al., 1999; Loubeyre et al., 1999). The transition from ice VII to X is also marked by a slight decrease in the unit cell volume.

The emerging planetary importance of high-pressure H₂O polymorphs in the formation and distinctiveness of H₂O-rich bodies, such as GJ 436 b, require H₂O-rich systems be studied in detail at pressures and temperatures likely in planetary interiors. At present, few data exist on the effects of impurities on the bonding and unit cell parameters of solid H₂O at high pressure, much less at elevated temperatures. Yet, for differentiated ice-rich bodies, there has likely been substantial interaction between hot H₂O-rich fluids and their rock components (McCord et al., 2001; Shock and McKinnon,

* Corresponding author. Tel.: +1 815 753 8395.

E-mail address: mfrank@niu.edu (M.R. Frank).

1993; Ransford et al., 1981; Scott et al., 2002). This study examined an H₂O-rich portion of the NaCl–H₂O system at high pressure and high temperature to provide an improved first-order approximation of impurity-rich high-pressure H₂O phases to be used in the next generation of phase stability and density profile models of H₂O-rich bodies. The NaCl–H₂O system was chosen due to its relative simplicity, well documented behavior over a large range of pressure and temperature, applicability to other ionic impurities, and as an extension of the room temperature, high-pressure work of Frank et al. (2006). Although the direct applicability of this system to a specific planetary body is limited, this study will serve as a good first-order approximation on the impacts of impurities on the equation of state and melting curve of high-pressure phases of H₂O and can be used as analogues for more complicated planetary systems.

2. Experimental and analytical methods

Presently, few data exist on the effects of impurities on H₂O at high pressure. Frank et al. (2006) presented a systematic study detailing the influence of charged species, Na⁺ and Cl[−], on the unit cell and OH bond length of ice VII. Based on the combination of the Raman and X-ray diffraction data, they hypothesized that the incorporation of those ions into ice VII resulted in a partial ordering of the protons by interionic attractions (Na⁺ with O and Cl[−] with H), which resulted in a transition to an ice X-like structure, where the protons are equidistant between the oxygen atoms (Frank et al., 2006). However, their work was restricted to room temperature and, hence, did not cover a large enough *PT* range for confident application to planetary systems. We hypothesize that the incorporation of Na⁺ and Cl[−] into ice VII will have only a minimal impact or slightly decrease the thermal expansion of ice VII, possibly through increased interionic attractions, but will decrease the melting temperature by increasing the Gibbs free energy of mixing. This study sought to test these hypotheses by examining the influence of Na⁺ and Cl[−] on the thermal expansion of ice VII and its melting curve. Ionic impurities that are more likely to be present in these planetary bodies, such as MgSO₄·*n*H₂O and NH₃, will be examined in future studies.

2.1. Experimental design

All experiments in this study were conducted by using externally heated Hydrothermal Diamond Anvil Cells, HDAC, designed by William A. Bassett (Bassett et al., 1993). The diamond anvils had 350 μm culets, were approximately 2 mm in length from the table to the culet, and were mounted on tungsten carbide seats using Resbond 940 brand cement. The gasket material was rhenium with an original thickness of 400 μm that was pre-indented to 40–60 μm. Sample chambers of 150 μm diameters were drilled in the compressed regions by using an EDM so that the holes acted as sample chambers bound on the sides by the gaskets and between the diamond anvils. Five weight percent, 1.60 mol%, NaCl aqueous solutions were prepared by dissolving crystalline NaCl (assay, anhydrous basis ≥99.0%) in deionized H₂O (>16.7 MΩ). The aqueous solutions were loaded into the sample chamber along with approximately ten 5–10 μm flakes of gold, used as a pressure indicator (Alfa Aesar[®] stock # 42154, lot # B13L23), and compressed, at room temperature, to seal the contents in the sample chamber. Each heating cycle utilized a separate sample loading and no runs were preheated.

Heating was achieved by passing current through chromel wires wrapped around the tungsten carbide seats of each diamond. High temperatures were obtained by using three variable transformers.

A main 20 A maximum transformer controlled two 10 A maximum transformers that were connected separately to each heater of the HDAC. Temperatures were monitored with type-K thermocouples placed directly against the surface of each diamond. Temperatures were kept within 5 K of the set temperature during data collection. Argon–hydrogen (1% hydrogen) gas was allowed to flow over the diamonds and the heaters to prevent corrosion during high-temperature operation.

2.2. Analytical methods: X-ray diffraction

All experiments were conducted at the GSECARS 13-BM-D beamline at the Advanced Photon Source, Argonne National Laboratory. An angle dispersive X-ray diffraction technique using monochromatic X-ray radiation, 0.3344 Å, and a MAR345 online imaging system were used to analyze the powder X-ray diffraction lines of the sample as a function of pressure and temperature. The X-ray beam was 14 and 7 μm in the horizontal and vertical directions, respectively, and was rastered across the sample chamber to search for all phases present in the chamber and to minimize the effects of ice grain coarsening. Data were analyzed using the FIT2D software package (Hammersley, 1997). FIT2D software and a known calibrant, CeO₂, were utilized to calibrate the sample to detector distance, coordinates of the directed beam on the detector, and the angle and tilt of the detector. There was little to no overlap of the main diffraction lines for ice VII, halite and gold over the majority of the pressure and temperature range of this study. The unit cell parameter of gold, determined from the diffraction lines, was used in conjunction with the previously established Anderson et al. (1989) *PVT* equation of state (*EoS*) to estimate the experimental pressure. Although there are more recent *EoS* for gold (Fei et al., 2004, 2007; Shim et al., 2002), we chose to use Anderson et al. (1989) to maintain an internal consistency with previous studies on pure ice VII at high temperature (Fei et al., 1993; Frank et al., 2004) and the room temperature work on NaCl-doped ice VII (Frank et al., 2006). Variations in the gold unit cell volume calculated from the {1 1 1}, {2 0 0}, {2 2 0}, {3 1 1}, and {2 2 2} diffraction lines were monitored and used to assess deviatoric stresses in the non-hydrostatic diamond anvil cell (Meng et al., 1993). The uncertainty in the unit cell parameter for gold, and thus the calculated pressure, was propagated through the pressure calculation to provide a minimum pressure uncertainty.

3. Results

Frank et al. (2006) hypothesized that impurities can affect the properties of high-pressure H₂O polymorphs in H₂O-rich bodies and icy satellites. They examined the phase relations, OH stretching frequencies and unit cell parameters of ice VII samples doped with Na⁺ and Cl[−] by using a diamond anvil cell (DAC) with Raman spectroscopy and synchrotron X-ray diffraction. This study extended the work of Frank et al. (2006) to include the effects of Na⁺ and Cl[−] on the thermal expansivity and melting curve of ice VII at conditions of planetary interiors. Diffraction data were collected up to 800 K and 32 GPa and compared to the 298 K data from Frank et al. (2006) and the numerous studies on ice VII formed from pure H₂O (Hemley et al., 1987; Fei et al., 1993; Datchi et al., 2000; Wolanin et al., 1997; Lin et al., 2004; Dubrovinskaia and Dubrovinsky, 2003; Frank et al., 2004). Our highest-pressure experiments are limited to less than 450 K because the gasket failed during heating from 450 to 500 K.

3.1. X-ray diffraction

Powder diffraction patterns of gold (the pressure standard) and ice VII formed from pure H₂O (Fig. 1) and 5 wt.% NaCl aqueous

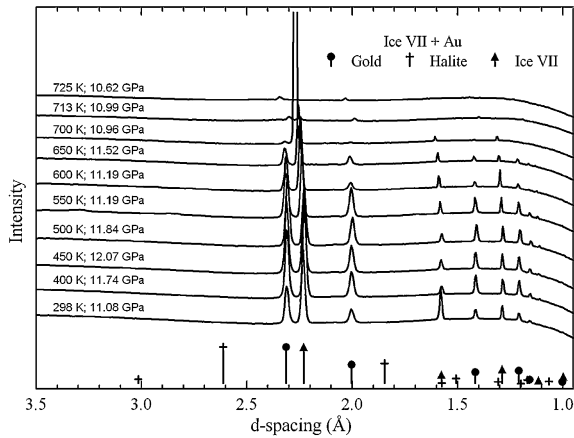


Fig. 1. Diffraction patterns of ice VII (+ gold as a pressure marker) formed from pure H₂O. Sticks with crosses, circles and triangles represent diffraction lines of halite, gold and ice VII, respectively. Ice VII diffraction lines were observed at 713 K and 11.0 GPa, but were absent at 725 K and 10.6 GPa. Thus, the melting point of ice VII was estimated as 719 ± 6 K and 10.8 ± 0.2 GPa where the uncertainty is defined as the midpoint between ice present and absent points in *PT* space. These data have not been smoothed.

solutions (Figs. 2 and 3) were obtained at room temperature up to 11.1 ± 0.3 and 26.6 ± 0.4 GPa, respectively. The {111}, {200}, {220}, {311} and {222} diffraction lines of gold used to calculate pressure were observed in all experiments. Slight variations in the unit cell parameter associated with {200} for gold suggest that there was only minimal deviatoric stress at 298 K. X-ray diffraction patterns of pure ice VII were characterized by the {110}, {200}, and {210} diffraction lines in all patterns and the {220} and {310} lines in approximately 80% of collected patterns. These diffraction lines were used to calculate the unit cell parameter and volume of ice VII (Table 1). No diffraction lines indicative of halite or any NaCl phase(s) were recorded at 298 K (Figs. 1–3) in ice VII formed from either the pure H₂O or the 5 wt.% NaCl aqueous solution.

3.2. Isothermal compression of ice VII at 298 K

Ice VII was compressed at 298 K up to the target pressure prior to heating and the {110}, {200}, {210}, {220} and {310} diffrac-

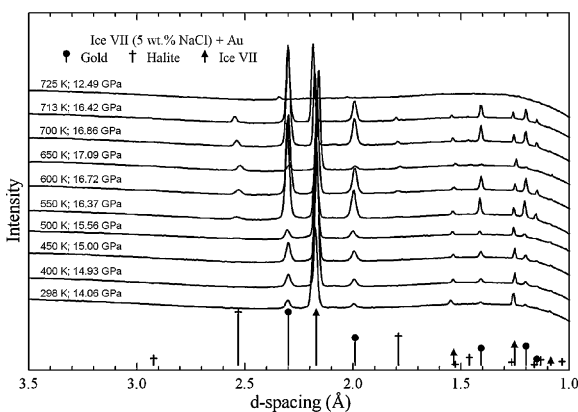


Fig. 2. Diffraction patterns of ice VII (+ gold as a pressure marker) formed from a 5 wt.% NaCl aqueous solution. Sticks with crosses, circles and triangles represent diffraction lines of halite, gold and ice VII, respectively. Halite diffraction lines became discernible as the sample temperature reached 500 K and also developed into more intense and defined peaks as the temperature was raised to the melting point of the high-pressure ice. The melting point of ice VII was estimated as 719 ± 6 K and 14 ± 2 GPa with the large uncertainty in pressure resulting from a drop in pressure during melting. These data have not been smoothed.

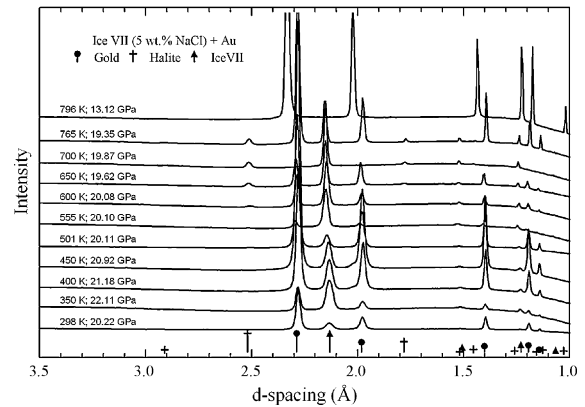


Fig. 3. Ice VII (+ gold as a pressure marker) formed from a 5 wt.% NaCl aqueous solution. Sticks with crosses, circles and triangles represent diffraction lines of halite, gold and ice VII, respectively. Halite diffraction lines became discernible as the sample temperature reached 501 K and also developed into more intense and defined peaks as the temperature was raised to the melting point of the high-pressure ice. The melting point of ice VII was estimated as 780 ± 16 K and 16 ± 3 GPa where the uncertainty is defined as the midpoint between ice present and absent points in *PT* space. These data have not been smoothed.

tion lines of ice VII were used to calculate its unit cell parameters where possible (Table 1). The 298 K compression data were collected up to 11.1 ± 0.3 and 26.6 ± 0.4 GPa for pure ice VII and ice VII formed from a 5 wt.% NaCl–H₂O solution, respectively. *PVT* data show that the ice VII formed from pure H₂O in this study is consistent with the 298 K data from previous studies (Hemley et al., 1987; Fei et al., 1993; Frank et al., 2004). The data from these studies were fit to third-order Birch–Murnaghan *EoS*:

$$P \text{ (GPa)} = \frac{3}{2} K_{T0} \left[\left(\frac{V_0}{V} \right)^{7/3} - \left(\frac{V_0}{V} \right)^{5/3} \right] \times \left[1 - \frac{3}{4} (4 - K'_{T0}) \left(\left(\frac{V_0}{V} \right)^{2/3} - 1 \right) \right] \quad (1)$$

where K_{T0} , K'_{T0} and V_0 are the isothermal bulk modulus, its pressure derivative and the volume at zero pressure, respectively (Birch, 1978; Table 2). The pure H₂O compression datum presented in this study matches closely the value predicted from these models. Additionally, data at 298 K for the ice VII doped with Na⁺ and Cl⁻ match closely the data and *EoS* outlined by Frank et al. (2006) using the same formulation for the *EoS*. The results indicated ice VII formed from a 5 wt.% NaCl-bearing aqueous solution has a unit cell volume which is depressed systematically by approximately 5% relative to ice VII formed from H₂O only (Fig. 4).

3.3. Phase stability as a function of temperature

All diffraction lines in the pure ice VII samples can be indexed with ice VII (Fig. 1) whereas high-temperature data for ice VII formed from a 5 wt.% NaCl–H₂O solution (Figs. 2 and 3) exhibit a remarkable trend. Ice formed from a NaCl-bearing aqueous solution at pressures greater than 2.2 GPa and less than 500 K can be indexed by ice VII only. Additionally, optical observations indicated that the sample was composed of only two phases (ice VII and gold). However, at temperatures greater than 500 K, diffraction lines indicative of halite (NaCl) are observed and become more intense with increasing temperature and only disappear at the melting point of the high-pressure ice. This phenomenon was observed in all NaCl-bearing ice samples that were heated to greater than 500 K. X-ray scans of the entire sample chamber at temperatures greater than the melting temperature of the ice VII showed

Table 1

Pressure, volume and temperature data for ice VII formed from pure H₂O and a 5 wt.% NaCl–H₂O solution

Ice VII			
Temperature (K)	Pressure (GPa)	Lattice parameters (Å)	Volume (Å ³)
NaCl–H ₂ O			
298 ± 2	4.8 ± 0.3	3.2433 ± 0.0024	34.12 ± 0.08
350 ± 5	4.6 ± 0.1	3.2505 ± 0.0010	34.34 ± 0.03
400 ± 5	4.5 ± 0.2	3.2583 ± 0.0021	34.59 ± 0.07
450 ± 5	4.9 ± 0.1	3.2564 ± 0.0026	34.53 ± 0.08
463 ± 12	4.4 ± 0.5	Melting point	Melting point
475 ± 5	4.0 ± 0.1	Fluid NaCl–H ₂ O	
NaCl–H ₂ O			
298 ± 2	20.2 ± 0.3	3.0059 ± 0.0018	27.16 ± 0.05
350 ± 5	22.1 ± 0.2	2.9888 ± 0.0021	26.70 ± 0.06
400 ± 5	21.2 ± 0.3	3.0011 ± 0.0035	27.03 ± 0.09
450 ± 5	20.9 ± 0.3	3.0066 ± 0.0041	27.18 ± 0.11
501 ± 5	20.1 ± 0.2	3.0188 ± 0.0026	27.51 ± 0.07
555 ± 5	20.1 ± 0.2	3.0239 ± 0.0022	27.65 ± 0.06
600 ± 5	20.1 ± 0.4	3.0322 ± 0.0047	27.88 ± 0.13
650 ± 5	19.6 ± 0.2	3.0433 ± 0.0039	28.19 ± 0.11
700 ± 5	19.9 ± 0.2	3.0499 ± 0.0022	28.37 ± 0.06
765 ± 5	19.4 ± 0.3	3.0678 ± 0.0042	28.87 ± 0.12
780 ± 16	16 ± 3	Melting point	Melting point
796 ± 5	13.1 ± 0.3	Fluid NaCl–H ₂ O	
NaCl–H ₂ O			
298 ± 2	14.1 ± 0.4	3.0766 ± 0.0031	29.12 ± 0.09
400 ± 5	14.9 ± 0.5	3.0699 ± 0.0025	28.93 ± 0.07
450 ± 5	15.0 ± 0.3	3.0736 ± 0.0066	29.03 ± 0.19
500 ± 5	15.6 ± 0.4	3.0717 ± 0.0024	28.98 ± 0.07
550 ± 5	16.4 ± 0.3	3.0682 ± 0.0031	28.88 ± 0.09
600 ± 5	16.7 ± 0.2	3.0713 ± 0.005	28.97 ± 0.02
650 ± 5	17.1 ± 0.1	3.0732 ± 0.0044	29.03 ± 0.12
700 ± 5	16.9 ± 0.3	3.0884 ± 0.0062	29.46 ± 0.18
713 ± 5	16.4 ± 0.3	3.0957 ± 0.0036	29.67 ± 0.10
719 ± 6	14 ± 2	Melting point	Melting point
725 ± 5	12.5 ± 0.3	Fluid NaCl–H ₂ O	
NaCl–H ₂ O			
298 ± 2	26.6 ± 0.4	2.9483 ± 0.0018	25.63 ± 0.05
400 ± 5	31.7 ± 0.4	2.9113 ± 0.0025	24.68 ± 0.06
450 ± 5	32.0 ± 0.4	2.9104 ± 0.0040	24.65 ± 0.10
Pure H ₂ O			
298 ± 2	11.1 ± 0.3	3.1450 ± 0.0043	31.11 ± 0.13
400 ± 5	11.7 ± 0.4	3.1383 ± 0.0026	30.91 ± 0.08
450 ± 5	12.1 ± 0.4	3.1390 ± 0.0034	30.93 ± 0.10
500 ± 5	11.8 ± 0.4	3.1481 ± 0.0017	31.20 ± 0.05
550 ± 5	11.2 ± 0.3	3.1647 ± 0.0033	31.70 ± 0.10
600 ± 5	11.2 ± 0.4	3.1726 ± 0.0038	31.93 ± 0.11
650 ± 5	11.5 ± 0.4	3.1748 ± 0.0022	32.00 ± 0.07
700 ± 5	11.0 ± 0.4	3.2004 ± 0.0040	32.78 ± 0.12
713 ± 5	11.0 ± 0.2	3.2032 ± 0.0056	32.87 ± 0.17
719 ± 6	10.8 ± 0.2	Melting point	Melting point
725 ± 5	10.6 ± 0.2	Fluid H ₂ O	

Gold was used as a pressure marker and the pressure was obtained from the gold unit cell parameter. The melting point is defined as the midpoint between ice present and ice absent points in *PT* space. Please refer to the text for a discussion of uncertainty.

no halite grains were present in the high-temperature fluid. The experiment which was conducted at approximately 4–4.5 GPa displayed ice-melting at less than 500 K and did not produce any halite diffraction lines. All experimental runs produced homogenous ice samples and no halite crystals were observed in the sample chamber after quench.

3.4. Thermal expansion of ice VII

Pressure–volume data were also collected at elevated temperatures, up to the melting point of the high-pressure ice (Figs. 1–3). The observed expansion of the unit cell volumes in this study was determined by comparing the volume of ice VII at elevated temperatures to the 298 K compression models of Fei et al. (1993) and

Frank et al. (2006) for pure and NaCl-doped ice VII, respectively. Rather than refit the pure ice VII data presented in this study, we compared our data to the model values from Fei et al. (1993). They utilized the volume coefficient of thermal expansion $\alpha(P, T)$ defined as

$$\alpha(P, T) = \alpha_0(T) \left[1 + \left(\frac{K'_{T0}}{K_{T0}} \times P \right)^{-\eta} \right] \quad (2)$$

where $\alpha_0(T)$ is the zero-pressure thermal expansion coefficient and η is an adjustable parameter of the pressure effect on the measured volume and was calculated to be 0.9. Fei et al. (1993) noted that $\alpha_0(T)$ could be expressed as

$$\alpha_0(T) = a_0 + a_1 T \quad (3)$$

where a_0 and a_1 are empirical coefficients and were determined to be -4.1×10^{-4} and $1.54 \times 10^{-6}/\text{K}$, respectively. The equation of state model of Fei et al. (1993) correlates closely with the high- and high-temperature data presented in this study for pure ice VII.

Model parameters for the volume coefficient of thermal expansion were also calculated for NaCl-doped ice VII from the data presented in this study. Whereas the 298 K *EoS* from Fei et al. (1993) was used for the pure ice VII data of this study, the 298 K *EoS* outlined in Frank et al. (2006) was employed to model ice VII with incorporated Na⁺ and Cl⁻. The V_0 , K_{T0} , and K'_{T0} were $39.1 \pm 0.1 \text{ \AA}^3$, $26.2 \pm 1.4 \text{ GPa}$, and 4.1 ± 0.2 , respectively. The thermal expansion of ice VII formed from a 5 wt.% NaCl aqueous solution was addressed using the procedure outlined in Fei et al. (1993) and produced a model where η , a_0 , and a_1 were found to be 0.9, -4.1×10^{-4} and $1.54 \times 10^{-6}/\text{K}$, respectively. The *PVT* data match closely the predicted values (Fig. 5). The data from pure and NaCl-doped ice VII indicate that the unit cell of ice VII expanded systematically with increasing temperature. The exsolution of halite at high temperatures did not change appreciably the thermal expansion coefficient for the ice phase, and suggests the exsolved NaCl probably represents only a small proportion of the Na⁺ and Cl⁻ in the ice VII structure.

3.5. Ice VII melting curve

The disappearance of the diffraction pattern of ice VII along with the appearance of diffuse scattering was used to monitor

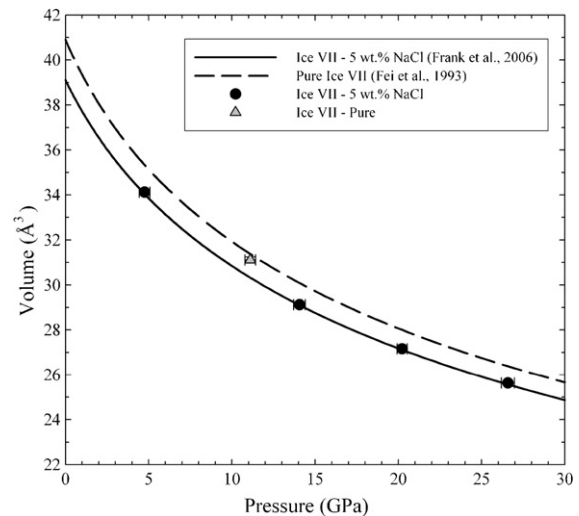


Fig. 4. The 298 volumetric data of ice VII samples as a function of pressure compared favorably to the compression models of Frank et al. (2004) and Fei et al. (1993) for ice VII formed from pure H₂O (gray triangle) and 5 wt.% NaCl aqueous solutions (black circles), respectively.

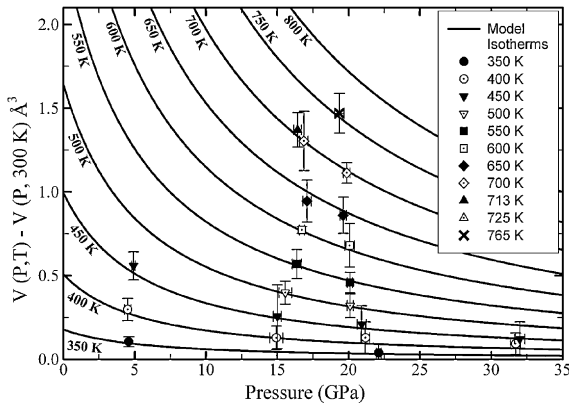


Fig. 5. The difference between the $V(P, T)$ – volume, \AA^3 , at pressure and temperature and the $V(P, 300\text{ K})$ – volume, \AA^3 , at elevated pressure with temperature fixed at 300 K for ice VII samples formed from a 5 wt.% NaCl aqueous solution is displayed as a function of pressure and temperature. The thermal expansion model was constructed by obtaining $V(P, 300\text{ K})$ from the Frank et al. (2006) model and the thermal expansion coefficients for pure ice VII from Fei et al. (1993). The data indicate that the thermal expansion coefficients for pure and NaCl-doped ice VII are similar within the uncertainty of our data.

melting. The melting point was defined by the midpoint between ice VII present and absent points in PT space. The pure H_2O ice melting data of this study are indistinguishable from the data and models of Lin et al. (2004) and Datchi et al. (2000), whereas the work of Dubrovinskaia and Dubrovinsky (2003) and Frank et al. (2004) underestimate the melting point. The three melting points for ice VII formed from a 5 wt.% NaCl aqueous solution (Fig. 6) were

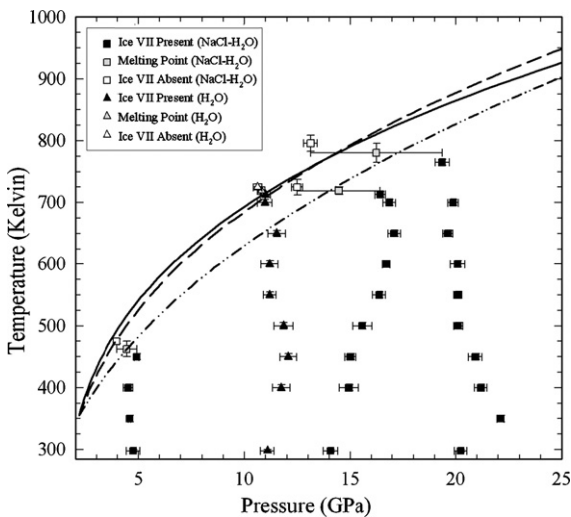


Fig. 6. The diffraction lines of ice VII formed from pure H_2O (triangles) were monitored as a function of pressure and temperature up to the melting temperature at any given pressure. The methodology employed in this study was to use the disappearance of the diffraction pattern of ice VII. The melting curve was defined by the midpoint (gray triangle and circle) between ice VII present (black symbols) and absent points (open symbols) in pressure–temperature space. The melting point determined for pure ice VII matches closely the work of Lin et al. (2004), solid line, and Datchi et al. (2000), dashed line, whereas the work of Dubrovinskaia and Dubrovinsky (2003) and Frank et al. (2004) underestimate the melting point. The melting points of ice VII formed from a 5 wt.% NaCl aqueous solution (squares) are defined by the midpoints between ice-present (black squares) and ice-absent (open squares) points in PT space. A melting curve was estimated by using the Simon–Glatzel equation (dash–dot–dot line) using the three data points and the ice VI, ice VII, liquid–water triple point (2.17 GPa and 355 K) for the pure H_2O system. The melting points and the calculated melting curve occur at lower temperatures than the pure ice VII data of this study and the data and models of Lin et al. (2004) and Datchi et al. (2000).

used to establish a melting curve for NaCl-doped ice by using the Simon–Glatzel equation (Simon and Glatzel, 1929):

$$\frac{P - P_t}{P_c} = \left(\frac{T}{T_t} \right)^\alpha - 1 \quad (4)$$

where P and T are the pressure and temperature along the melting curve, P_t and T_t are the pressure and temperature at the ice VI, ice VII, liquid–water triple point (2.17 GPa and 355 K, respectively), and P_c (2.421) and α (2.511) are the best-fit parameters. The calculated curve for ice VII doped with NaCl using this methodology is consistent with the data of this study (Fig. 6). The low number of melting point data and the associated large uncertainties make extrapolation of the determined melting curve to pressures greater than 25 GPa imprudent.

The results for ice VII formed from a 5 wt.% NaCl– H_2O solution illustrate that melting occurred at lower temperatures, by approximately 40 K, than would be expected for pure ice VII (Fig. 6). A strong correlation of the pure ice VII melting point determined in this study with previous workers (Lin et al., 2004; Datchi et al., 2000) suggests the difference in melting temperature is inherent to the NaCl– H_2O system rather than a product of experimental or analytical errors. Further, our lowest temperature melting point datum for NaCl-doped ice, where halite exsolution was not observed, implies that the melting point depression was not a result of melting at grain boundaries between halite and ice VII. These data suggest that the presence of Na^+ and Cl^- in the ice VII structure results in a depression of the ice VII melting curve at any given pressure even with the large melting point uncertainty. Also of note, the exsolution of a small proportion of Na^+ and Cl^- to form halite did not seem to influence significantly the melting point of the Na^+ - and Cl^- -doped ice VII phase.

4. Discussion

Frank et al. (2006) hypothesized that impurities can affect the properties of high-pressure H_2O polymorphs in H_2O -rich bodies and icy satellites. Ice VII formed from a 5 wt.% NaCl aqueous solution at 298 K has been shown to produce a single homogenous solid phase (Frank et al., 2006). They suggested that the dissociation of NaCl in aqueous solutions results in Na^+ and Cl^- being incorporated into high-pressure phases of H_2O and, further, they estimated the maximum impurity concentration was 7.5 ± 2.5 wt.% NaCl by monitoring diffraction lines, Raman spectra and using optical evidence. The incorporation of Na^+ and Cl^- into the ice VII structure increased the density and bulk modulus by up to 5% and 10–20%, respectively. This study sought to disprove the hypothesis of Frank et al. (2006) and characterize the NaCl– H_2O system at high pressures and high temperatures.

The diffraction data presented in this study confirm the findings of Frank et al. (2006) that Ice VII formed from a 5 wt.% NaCl aqueous solution at 298 K will produce a single homogenous solid phase (Figs. 2 and 3). Compression of this phase to 26.6 ± 0.4 GPa did not produce any new diffraction lines and also supports the compression curve detailed in Frank et al. (2006).

4.1. Immiscibility in the NaCl– H_2O system at high pressure

Ice VII, stable from 2.2 to 62 GPa, has a body-centered cubic structure with partially ordered protons. Ice X is stable at pressures greater than 62 GPa (Pruzan et al., 1997; Goncharov et al., 1999) at room temperature and only differs from ice VII in that its protons are ordered and equidistant between the oxygen atoms. Frank et al. (2006) hypothesized, based on a study restricted to room temperature, that Na^+ and Cl^- could be incorporated into the ice VII structure with the Na^+ and Cl^- residing in the FCC sites of the BCC

ice VII structure. This, they suggested, would result in an increase in the ordering of the protons through interionic attractions (Na^+ with O and Cl^- with H), which could result in a transition to an ice X-like structure. High-temperature diffraction data from the study presented here suggest that the single, homogenous ice VII phase with 5 wt.% NaCl incorporated into its structure (as Na^+ and Cl^-) undergoes unmixing upon heating at approximately 500 K. As this single, homogenous phase was heated from room temperature to 500 K, a second phase, halite, was produced. The appearance of halite upon heating cannot be interpreted solely as a result of an expansion of the halite liquidus with increasing pressure because the required phase progression during melting is not supported by our data.

The unmixing phenomenon may be a consequence of enthalpy, which takes into account the PV part of the Gibbs free energy equation, becoming dominant. However, since the phase exsolution occurs at approximately 500 K over a range of pressure (15–20 GPa), this explanation is not well supported by the available data. Conversely, an increase in entropy typically accompanies an increase in temperature, and since entropy is a measure of possible energy and matter configurations, it is possible that heating produced increased disorder within the ice VII structure. This increase in disorder reverses the ordering forced on the ice VII protons by the incorporation of Na^+ and Cl^- and results in the structure reverting back to the partially ordered state of pure ice VII. In other words, proton ordering was forced partially by adding the charged species and now it is being reversed by the increase in entropy which is causing some of the Na^+ and Cl^- ions to be expelled from the ice VII structure and form halite. Depression of the melting point (and increasing intensity of halite diffraction lines with increasing temperature) observed in ice VII formed from the NaCl aqueous solution suggests that not all Na^+ and Cl^- ions were exsolved and that some Na^+ and Cl^- ions were still within the high-pressure ice structure up to the melting point. Similar immiscibility phenomena with increasing temperature include nicotine–water, methyl ethyl ketone–water, and diethylamine–water (Glasstone, 1946). These systems have “lower” consolute temperatures that represent a decrease in solubility with increasing temperature. The consolute temperatures are hypothesized to represent a response to the formation of a new compound, often, this new compound is connected with the presence of a hydrogen bond. The ice VII–ice X transition is defined by proton ordering and we hypothesize that the Cl^- and H^+ ionic interaction is at the heart of the variance in ice VII properties. It should be noted that the systems listed by Glasstone (1946) are all liquid–liquid systems and may not be comparable directly to the solid ice VII–halite system.

4.2. Ice VII melting

The melting curve for ice VII formed from pure H_2O agrees exceptionally well with the data and models of Lin et al. (2004) and Datchi et al. (2000), whereas the work of Fei et al. (1993), Dubrovinskaia and Dubrovinsky (2003) and Frank et al. (2004) underestimate the melting temperature over a large range of pressure (Fig. 6). The data presented in this paper are the first diffraction-based data that supports the Raman-spectroscopic based work of Lin et al. (2004) and Datchi et al. (2000). The studies of Fei et al. (1993) and Frank et al. (2004) were conducted using Mao-Bell style diamond anvil cells and energy dispersive X-ray techniques. It is possible that a systematic error is introduced through the design of the cells, thermocouple chosen, or placement of thermocouple; however, the strong agreement in the thermal expansion coefficient between this study and the Fei et al. (1993) and Frank et al. (2004) studies argues against any cell design problems. The most likely source for the discrepancy is the use of an energy dispersive technique which could provide false melting

points through the growth of large single crystals that would be difficult to detect using this technique. This study, using an angle dispersive technique, noted a coarsening of the ice sample near the melting point which, although observable with the angle dispersive technique, may appear to be the disappearance of diffraction lines and interpreted as melting when using energy dispersive analytical methods. Dubrovinskaia and Dubrovinsky (2003) used angle dispersive techniques and an elaborate heating system with excellent control and stability. Although our data suggest that they underestimate the melting point of ice VII, the discrepancy is slight and may be due to variations in the EoS for gold used to estimate pressure in this study.

The addition of Na^+ and Cl^- to ice VII lowered systematically the melting point of NaCl-doped ice VII (Fig. 6) relative to the pure ice VII data from this study and the studies of Lin et al. (2004) and Datchi et al. (2000). Although Na^+ and Cl^- were observed to exsolve from the ice phase, the melting data suggest that the presence of Na^+ and Cl^- in the ice VII structure results in a depression of the melting curve. The melting point data at approximately 4 GPa imply that the melting point depression was not a result of melting at grain boundaries because halite exsolution was not observed in that experiment. Thus, Na^+ and Cl^- incorporation must lower the Gibbs free energy of formation for ice VII through mixing phenomena or through contact with the exsolved NaCl-rich phase.

4.3. Planetary implications

Data from the Galileo and Cassini missions greatly increased the quality and quantity of data on ice-rich bodies and have been used extensively to produce a wide range of interior models to explain the moment of inertia and density data and their formation and evolution (e.g. Anderson et al., 1996, 1998; Kuskov and Kronrod, 2001; Sohl et al., 2002). Proposals for the accretion and differentiation of these bodies suggest that the ice, silicate and iron-dominated portions of the bodies, although segregated currently, interacted over a large range of pressure and temperature in the past (Scott et al., 2002). Induced magnetic fields have been detected during close encounters and interpreted as emanating from relatively shallow portions of the icy bodies (Khurana et al., 1998; Zimmer et al., 2000; Kivelson et al., 2000, 2002). Hypotheses have been formulated suggesting that shallow, subsurface oceans with low to moderate salinities could explain these relatively shallow magnetic fields (e.g., McKinnon, 1999; Klemaszewski and Greeley, 2001; Ruiz, 2001). Any interactions of the deeper ice and rock portions of the body with this solute-bearing fluid over the course of the body's history will most likely result in the incorporation of impurities into the high-pressure ices.

Frank et al. (2006) demonstrated that, for Callisto, the increase in density of ice VII formed from a NaCl-bearing solution will increase the outer, low-pressure ice and fluid layer thickness by approximately 70 km due to the compaction of the ice VII rich-layer. Their study was limited to room temperature, and so its applicability is also limited. The study presented here illustrates that the density of NaCl-doped ice VII will be higher relative to pure ice VII at elevated temperatures and implies that the density of ice layers within a body such as Callisto need to be evaluated based on their possible impurities.

The exsolution of halite from the NaCl-doped ice VII suggests that temperature or pressure-induced phase transitions, much like the upper to lower-mantle transition within Earth, are possible at depth within ice-rich bodies. Halite exsolution from Na^+ - and Cl^- -bearing ice VII promotes a self-segregating layer or zone deep within ice-rich bodies (Fig. 7). Although chlorides are not thought to be abundant on these bodies, our work allows for general conclusions about ionic impurities and their impact on the behavior of

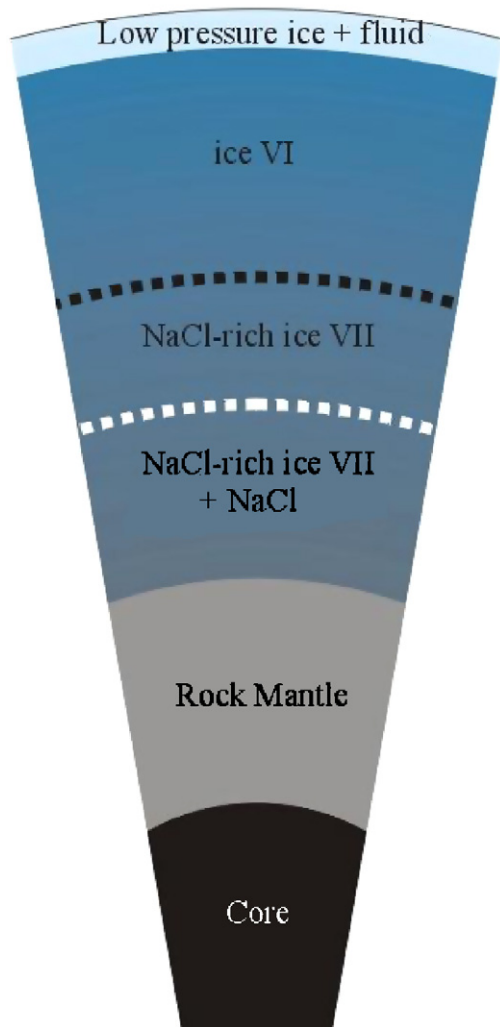


Fig. 7. A hypothetical H₂O-rich planet is represented here with an outer layer of low-pressure ice with underlying solute-rich fluid. The fluid crystallizes under increasing pressure to ice VI and transitions to an impurity-rich (NaCl in this example) ice VII at approximately 2.2 GPa. This hypothetical planet has a deeper rock (hydrous) mantle overlying a Fe- or rock-rich core. Our data suggests that at temperature greater than 500 K, the Na and Cl contained within the ice VII will begin to exsolve out and form a two phase mixture of halite plus ice VII (with remnant Na⁺ and Cl⁻). Although our work is limited to the NaCl–H₂O system, other ionic impurities in high-pressure phases of H₂O may behave similarly. Solute-bearing aqueous vents, unexplained domes, and/or salt-rich regions on the surface of H₂O-rich planetary bodies may be a result of this self-segregating layer caused by the unmixing of ionic impurities from the impurity-bearing ice VII.

high-pressure phases of H₂O. If similar exsolution occurs in other impurity-rich H₂O systems, this zone could initiate the formation of solute-rich “melt” pockets that will influence the rheologic properties (e.g. Durham et al., 1996; Kargel et al., 1991) of the ice and may encourage plume motion towards the surface. Surface manifestations of these plumes/diapirs could include solute-bearing aqueous vents, unexplained doming, and/or salt-rich regions (Kargel, 1991). Similar salt-rich zones have been observed on the surface of Europa and other icy bodies (McCord et al., 1998, 1999, 2001, 2002; Dalton et al., 2005).

Additionally, the presence of Na⁺ and Cl⁻ within ice VII systematically lowered the melting point of NaCl-doped ice VII relative to pure ice VII further limiting the *PT* stability field of NaCl-doped ice VII. The hypothesis of Frank et al. (2006) and the work of this study are only applicable to ice VII with charged impurities and should not be the same for neutral molecules or elements. Therefore, experi-

ments detailing the incorporation of other ionic impurities that are likely to be present in these planetary bodies, such as MgSO₄·*n*H₂O and NH₃, should be addressed in future studies along with associated compounds to further test the hypothesis of Frank et al. (2006) and the work presented in this study.

5. Conclusions

High-pressure phases of H₂O are of great importance in planetary physics. We examined an H₂O-rich portion of the NaCl–H₂O system at high pressures and high temperatures to ascertain the properties and behavior of impurity-rich ice VII. Although the direct applicability of this system to a specific planetary body is limited, this study will serve as a good first-order approximation on the impacts of impurities on the equation of state and melting curve of high-pressure phases of H₂O and can be used as analogues for more complicated planetary systems. The incorporation of Na⁺ and Cl⁻ into ice VII increased the density of the ice phase relative to pure ice VII over the entire range of pressure and temperature of this study. Whereas the thermal expansion of NaCl-doped ice VII was consistent with previous studies of pure ice VII, the melting curve of ice VII formed from a 5 wt.%, 1.60 mol%, NaCl–H₂O solution is systematically depressed relative to the melting curve of pure ice VII by approximately 40 K. This depression increased the stability field of fluid H₂O (at elevated pressures). The NaCl-bearing homogenous ice phase was observed to undergo unmixing at temperatures greater than 500 K. Diffraction lines indicative of halite (NaCl) are observed and become more intense with increasing temperature and only disappear at the melting point of the high-pressure ice. Phase unmixing combined with the depression of the NaCl-doped ice VII melting curve could promote the formation of a self-segregating layer or zone deep within ice-rich bodies. Thus, the exsolution of halite from the NaCl-doped ice VII at elevated temperatures may produce salt-rich diapirs that could generate salt-bearing aqueous vents and/or doming on H₂O-rich planetary bodies. The data presented in this study will allow for more precise and accurate density profile modeling of H₂O-rich bodies and provides an intriguing possible explanation for salt-rich surface features on select icy satellites.

Acknowledgements

This research was supported by the Research and Artistry Program at Northern Illinois University (MRF). Portions of this work were performed at GeoSoilEnviroCARS (Sector 13), Advanced Photon Source (APS), Argonne National Laboratory. GeoSoilEnviroCARS is supported by the National Science Foundation - Earth Sciences (EAR-0217473), Department of Energy - Geosciences (DE-FG02-94ER14466) and the State of Illinois. Use of the APS was supported by the U.S. Department of Energy, Basic Energy Sciences, Office of Science, under Contract No. W-31-109-Eng-38. We would like to thank F.J. Ryerson and an anonymous reviewer for helpful examinations of the manuscript.

References

- Anderson, J.D., Jacobson, R.A., McElrath, T.P., Moore, W.B., Schubert, G., Thomas, P.C., 2001. Shape, mean radius, gravity field, and interior structure of Callisto. *Icarus* 153, 157–161.
- Anderson, J.D., Lau, E.L., Sjogren, W.L., Schubert, G., Moore, W.B., 1996. Gravitational constraints on the internal structure of Ganymede. *Nature* 384, 541–543.
- Anderson, J.D., Lau, E.L., Sjogren, W.L., Schubert, G., Moore, W.B., 1997. Gravitational evidence for an undifferentiated Callisto. *Nature* 387, 264–266.
- Anderson, J.D., Schubert, G., Jacobson, R.A., Lau, E.L., Moore, W.B., Sjogren, W.L., 1998. Distribution of rock, metals, and ices in Callisto. *Science* 280, 1573–1576.
- Anderson, O.L., Isaak, D.G., Yamamoto, S., 1989. Anharmonicity and the equation of state for gold. *Journal of Applied Physics* 65, 1534–1543.

- Bassett, W.A., Shen, A.H., Bucknum, M., Chou, I.M., 1993. Hydrothermal studies in a new diamond anvil cell up to 10 GPa and from –190 to 1200 °C. *Pure and Applied Geophysics* 141, 487–496.
- Birch, F., 1978. Finite strain isotherm and velocities for single-crystal and polycrystalline NaCl at high pressures and 300 K. *Journal of Geophysical Research A* 83, 1257–1268.
- Brown, M.E., Calvin, W.M., 2000. Evidence for crystalline water and ammonia ices on Pluto's Satellite Charon. *Science* 287, 107–110.
- Butler, R.P., Vogt, S.S., Marcy, G.W., Fischer, D.A., Wright, J.T., Henry, G.W., Laughlin, G., Lissauer, J.J., 2004. A neptune–mass planet orbiting the nearby M Dwarf GJ 436. *Astrophysical Journal* 617, 580–588.
- Carlson, R.W., Smythe, W., Baines, K.H., Barbinis, E., Becker, K., Burns, R., Calcutt, S., Calvin, W.M., Clark, R.N., Danielson, G.E., Davies, A.G., Drossart, P., Encrenaz, Therese, Fanale, F.P., Granahan, J., Hansen, G., Herrera, P., Hibbitts, C., Hui, John, Irwin, P., Johnson, T. V., Kamp, L.W., Kieffer, H.H., Leader, F., Lellouch, E., Lopes-Gautier, Rosaly, Matson, D.L., McCord, T.B., Mehlman, R., Ocampo, A., Orton, G., Roos-Serote, M., Segura, M., Shirley, J., Soderblom, L., Stevenson, A., Taylor, F., Torson, J., Weir, A., Weissman, P., 1996. Near-infrared spectroscopy and spectral mapping of Jupiter and the Galilean satellites; results from Galileo's initial orbit. *Science* 274, 385–388.
- Consolmagno, G.J., Lewis, J.S., 1976. The evolution of icy satellite interiors and surfaces. *Icarus* 34 (2), 280–293.
- Dalton, J.B., Prieto-Ballesteros, O., Kargel, J.S., Jamieson, C.S., Jolivet, J., Quinn, R., 2005. Spectral comparison of heavily hydrated salts with disrupted terrains on Europa. *Icarus* 177, 472–490.
- Datchi, F., Loubeyre, P., LeToullec, R., 2000. Extended and accurate determination of the melting curves of argon, helium, ice (H₂O), and hydrogen (H₂). *Physical Review B* 61, 6535–6546.
- Dubrovinskaya, N., Dubrovinsky, L., 2003. Melting curve of water studied in externally heated diamond–anvil cell. *High Pressure Research* 23, 307–311.
- Durham, W.B., Stern, L.A., Kirby, S.H., 1996. Rheology of water ices V and VI. *Journal of Geophysical Research B: Solid Earth and Planets* 101, 2989–3001.
- Fei, Y., Li, J., Hirose, K., Minarik, W., Van Orman, J., Sanloup, C., van Westrenen, W., Komabayashi, T., Funakoshi, K., 2004. A critical evaluation of pressure scales at high temperatures by in situ X-ray diffraction measurements. *Physics of the Earth and Planetary Interiors* 143–144, 515–526.
- Fei, Y., Mao, H.K., Hemley, R.J., 1993. Thermal expansivity, bulk modulus, and melting curve of H₂O–Ice VII to 20 GPa. *Journal of Chemical Physics* 99, 5369–5373.
- Fei, Y., Ricolleau, A., Frank, M.R., Mibe, K., Shen, G., Prakapenka, V., 2007. Toward an internally consistent pressure scale. *Proc. Natl. Acad. Sci.* 104, 9182–9186, doi:10.1073/pnas.0609013104.
- Frank, M.R., Fei, Y., Hu, J., 2004. Constraining the equation of state of fluid H₂O to 80 GPa using the melting curve, bulk modulus and thermal expansivity of Ice VII. *Geochimica et Cosmochimica Acta* 68 (13), 2781–2790.
- Frank, M.R., Runge, C.E., Scott, H.P., Maglio, S.J., Olson, J., Prakapenka, V.B., Shen, G., 2006. Experimental study of the NaCl–H₂O system up to 28 GPa: implications for ice-rich planetary bodies. *Physics of the Earth and Planetary Interiors* 155, 152–162.
- Gillon, M., Pont, F., Demory, B.-O., Mallmann, F., Mayor, M., Mazeh, T., Queloz, D., Shporer, A., Udry, S., Vuissoz, C., 2007. Detection of transits of the nearby hot Neptune GJ 436 b. *Astronomy and Astrophysics* 472, L13–L16.
- Glasstone, S., 1946. *Textbook of Physical Chemistry*, second ed. D. Van Nostrand Company, New York, 1320 p.
- Goncharov, A.F., Struzhkin, V.V., Mao, H.K., Hemley, R.J., 1999. Raman spectroscopy of dense H₂O and the transition to symmetric hydrogen bonds. *Physical Review Letters* 83, 1998–2001.
- Greeley, R., Figueredo, P.H., Williams, D.A., Chuang, F.C., Klemaszewski, J.E., Kadel, S.D., Prockter, L.M., Pappalardo, R.T., Head III, J.W., Collins FG.C., Spaun, N.A., Sullivan, R.J., Moore, J.M., Senske, D.A., Tufts, B.R., Johnson, T.V., Belton, M.J.S., Tanaka, K.L., 2000. Geologic mapping of Europa. *Journal of Geophysical Research E: Planets* 105 (22), 578, 559–22.
- Greeley, R., Klemaszewski, J.E., Wagner, R., 2000b. Galileo views of the geology of Callisto. *Planetary and Space Science* 48, 829–853.
- Hammersley, A.P., 1997. FIT2D: an introduction and overview. ESRF Internal Report ESRF97HA02T.
- Head, J.W., Pappalardo, R., Collins, G., Belton, M.J.S., Giese, B., Wagner, R., Breneman, H., Spaun, N., Nixon, B., Neukum, G., Moore, J., 2002. Evidence for Europa-like tectonic resurfacing styles on Ganymede. *Geophysical Research Letters* 29, 1–4.
- Hemley, R.J., Jephcoat, A.P., Mao, H.K., Zha, C.S., Finger, L.W., Cox, D.E., 1987. Static compression of H₂O–ice to 128 GPa (1.28 mbar). *Nature* 330, 737–740.
- Kargel, J.S., 1991. Brine volcanism and the interior structures of asteroids and satellites. *Icarus* 94, 368–390.
- Kargel, J.S., Croft, S.K., Lunine, J.I., Lewis, J.S., 1991. Rheological properties of ammonia–water liquids and crystal–liquid slurries: planetological applications. *Icarus* 89, 93–112.
- Khurana, K.K., Kivelson, M.G., Stevenson, D.J., Schubert, G., Russell, C.T., Walker, R.J., Polansky, C., 1998. Induced magnetic fields as evidence for subsurface oceans in Europa and Callisto. *Nature* 395, 777–780.
- Kivelson, M.G., Khurana, K.K., Russell, C.T., Walker, R.J., Warnecke, J., Coroniti, F.V., Polansky, C., Southwood, D.J., Schubert, G., 1996. Discovery of Ganymede's magnetic field by the Galileo spacecraft. *Nature* 384, 537–541.
- Kivelson, M.G., Khurana, K.K., Russell, C.T., Volwerk, M., Walker, R.J., Zimmer, C., 2000. Galileo magnetometer measurements: a stronger case for a subsurface ocean at Europa. *Science* 289, 1340–1343.
- Kivelson, M.G., Khurana, K.K., Volwerk, M., 2002. The permanent and inductive magnetic moments of Ganymede. *Icarus* 157, 507–522.
- Klemaszewski, J.E., Greeley, R., 2001. Geological evidence for an ocean on Callisto. *Lunar and Planetary Science XXXII*, 1818.
- Kuskov, O.L., Kronrod, V.A., 2001. Core sizes and internal structure of Earth's and Jupiter's satellites. *Icarus* 151, 204–227.
- Lin, J.-F., Militzer, B., Struzhkin, V.V., Gregoryanz, E., Hemley, R.J., Mao, H.-k., 2004. High pressure–temperature Raman measurements of H₂O melting to 22 GPa and 900 K. *Journal of Chemical Physics* 121, 8423–8427.
- Loubeyre, P., LeToullec, R., Wolanin, E., Hanfland, M., Häusermann, D., 1999. Modulated phases and proton centering in ice observed by X-ray diffraction up to 170 GPa. *Nature* 397, 503–506.
- McCord, T.B., Hansen, G.B., Fanale, F.P., Carlson, R.W., Matson, D.L., Johnson, T.V., Smythe, W.D., Crowley, J.K., Martin, P.D., Ocampo, A., Hibbitts, C.A., Granahan, J.C., 1998. Salts on Europa's surface detected by Galileo's near infrared mapping spectrometer. *Science* 280, 1242–1245.
- McCord, T.B., Hansen, G.B., Matson, D.L., Johnson, T.V., Crowley, J.K., Fanale, F.P., Carlson, R.W., Smythe, W.D., Martin, P.D., Hibbitts, C.A., Granahan, J.C., Ocampo, A., 1999. Hydrated salt minerals on Europa's surface from the Galileo Near-Infrared Mapping Spectrometer (NIMS) investigation. *Journal of Geophysical Research* 104, 11827–11851.
- McCord, T.B., Hansen, G.B., Hibbitts, C.A., 2001. Hydrated salt minerals on Ganymede's surface: evidence of an ocean below. *Science* 292, 1523–1525.
- McCord, T.B., Teeter, G., Hansen, G.B., Sieger, M.T., Orlando, T.M., 2002. Brines exposed to Europa surface conditions. *Journal of Geophysical Research* 107, 1–6.
- McKinnon, W.B., 1999. Convective instability in Europa's floating ice shell. *Geophysical Research Letters* 26, 951–954.
- Meng, Y., Weidner, D.J., Fei, Y., 1993. Deviatoric stress in a quasi-hydrostatic diamond anvil cell: effect on the volume-based pressure calibration. *Geophysical Research Letters* 20, 1147–1150.
- Pruzan, P., Wolanin, E., Gauthier, M., Chervin, J.C., Canny, B., 1997. Raman scattering and X-ray diffraction of ice in the megabar range. Occurrence of symmetric disordered solid above 62 GPa. *Journal of Physical Chemistry* 101, 6230–6233.
- Ransford, G.A., Finnerty, A.A., Collerson, K.D., 1981. Europa's petrological thermal history. *Nature* 289, 21–24.
- Ruiz, J., 2001. The stability against freezing of an internal liquid–water ocean in Callisto. *Nature* 412, 409–411.
- Schenk, P.M., McKinnon, W.B., Gwynn, D., Moore, J.M., 2001. Flooding of Ganymede's bright, resurfaced terrains by low-viscosity water–ice lavas. *Nature* 410, 57–60.
- Shock, E.L., McKinnon, B.L., 1993. Hydrothermal processing of cometary volatiles–applications to Triton. *Icarus* 106, 464–477.
- Schubert, G., Zhang, K., Kivelson, M.G., Anderson, J.D., 1996. The magnetic field and internal structure of Ganymede. *Nature* 384 (6609), 544–545.
- Scott, H.P., Williams, Q., Ryerson, F.J., 2002. Experimental constraints on the chemical evolution of icy satellites. *Earth and Planetary Science Letters* 203, 399–412.
- Shim, S.-H., Duffy, T.S., Takemura, K., 2002. Equation of state of gold and its application to the phase boundaries near 660-km depth in Earth's mantle. *Earth and Planetary Science Letters* 203, 729–739.
- Simon, F.E., Glatzel, G., 1929. Bemerkungen zur Schmelzdruckkurve. *Zeitschrift für Anorganische und Allgemeine Chemie* 178, 309–316.
- Sohl, F., Spohn, T., Breuer, D., Nagel, K., 2002. Implications from Galileo observations on the interior structure and chemistry of the Galilean satellites. *Icarus* 157, 104–119.
- Wolanin, E., Pruzan, Ph., Chervin, J.C., Canny, B., Gauthier, M., Häusermann, D., Hanfland, M., 1997. Equation of state of ice VII up to 106 GPa. *Physical Review B* 56, 5781–5785.
- Zimmer, C., Khurana, K.K., Kivelson, M.G., 2000. Subsurface oceans on Europa and Callisto; constraints from Galileo magnetometer observations. *Icarus* 147, 329–347.